Chemical Science

ROYAL SOCIETY OF CHEMISTRY

EDGE ARTICLE

View Article Online
View Journal | View Issue

Cite this: *Chem. Sci.*, 2022, **13**, 3571

All publication charges for this article have been paid for by the Royal Society of Chemistry

Expanding the functionality of proteins with genetically encoded dibenzo[*b*,*f*][1,4,5]thiadiazepine: a photo-transducer for photo-click decoration†

Qin Xiong, Tingting Zheng, Xin Shen, Baolin Li, Jielin Fu, Xiaohu Zhao, Chunxia Wang and Zhipeng Yu *

Received 16th October 2021
Accepted 28th February 2022

DOI: 10.1039/d1sc05710c

rsc.li/chemical-science

Genetic incorporation of novel noncanonical amino acids (ncAAs) that are specialized for the photo-click reaction allows the precisely orthogonal and site-specific functionalization of proteins in living cells under photo-control. However, the development of a ring-strain *in situ* loadable dipolarophile (RILD) as a genetically encodable reporter for photo-click bioconjugation with spatiotemporal controllability is quite rare. Herein, we report the design and synthesis of a photo-switchable dibenzo[*b*,*f*][1,4,5]thiadiazepine-based alanine (DBTDA) ncAA, together with the directed evolution of a pyrrolysyl-tRNA synthetase/$tRNA_{CUA}$ pair (PylRS/$tRNA_{CUA}$), to encode the DBTDA into recombinant proteins as a RILD in living *E. coli* cells. The fast-responsive photo-isomerization of the DBTDA residue can be utilized as a converter of photon energy into ring-strain energy to oscillate the conformational changes of the parent proteins. Due to the photo-activation of RILD, the photo-switching of the DBTDA residue on sfGFP and OmpC is capable of promoting the photo-click ligation with diarylsydnone (DASyd) derived probes with high efficiency and selectivity. We demonstrate that the genetic code expansion (GCE) with DBTDA benefits the studies on the distribution of decorated OmpC-DBTD on specific *E. coli* cells under a spatiotemporal resolved photo-stimulation. The GCE for encoding DBTDA enables further functional diversity of artificial proteins in living systems.

Introduction

With many advances over the last two decades, click chemistry[1] has been increasingly exploited in the development of therapeutic agents,[2] the functionalization of materials,[3] and labelling biomacromolecules in living systems.[4] Taking into account its unique spatiotemporal controllability,[5] photo-click chemistry[6] has had a wide impact on a broad range of interdisciplinary research because of its utilization of photon energy[7] as well as the advantages of non-invasive manipulation.[8] To fulfill the stringent requirements for the purpose of bioorthogonal ligation, great efforts have been made to improve the photo-click strategy,[9] including the photo-induced 1,3-dipolar cycloaddition of tetrazole-alkene/alkyne systems,[10] photo-click chemistry between diarylsydnone (DASyd) and alkenes/alkynes,[11] light-triggered Diels–Alder reactions,[12] and photo-mediated strain promoted azide–alkyne cycloaddition (photo-SPAAC).[13] However, the diversity of bioorthogonal reporters dedicated to photo-click chemistry is quite limited (Scheme 1a).[14] This predicament has been addressed by the development of ring-strain *in situ* loadable dipolarophiles (RILDs)[15] to revive the concept of photo-activation (Scheme 1b).

Recently, our group reported a study regarding the photo-isomerization of a cyclic azobenzene, dibenzo[*b*,*f*]-[1,4,5]thiadiazepine (DBTD), and its ability to serve as a dipolarophile in cycloaddition with the nitrile imine generated from the photolysis of DASyd (Scheme 1c).[16] In fact, DBTD containing a cyclic azobenzene motif could swiftly respond to a programmable photo-stimulation sequence, transforming photon energy into ring-strain energy to accelerate the cycloaddition rate *in situ* (k_2, up to $1.6 \pm 0.16 \times 10^5$ M^{-1} s^{-1}). The excellent photo-switching and anti-fatigue performances of DBTD demonstrate a next-generation RILD reporter that is ultra-durable during complex photo-operations. However, its incorporation into proteins has been restricted within chemical approaches previously.

Genetic code expansion (GCE) with noncanonical amino acids (ncAAs, Scheme 1a) has emerged as an extremely powerful tool to incorporate artificial functionalities into engineered proteins in living systems.[17] Harbouring the unique chemical or

Key Laboratory of Green Chemistry and Technology of Ministry of Education, College of Chemistry, Sichuan University, 29 Wangjiang Road, Chengdu, 610064, P. R. China. E-mail: zhipengy@scu.edu.cn

† Electronic supplementary information (ESI) available: Containing details on experimental procedures, spectra properties, and characterization of all new compounds. See DOI: 10.1039/d1sc05710c

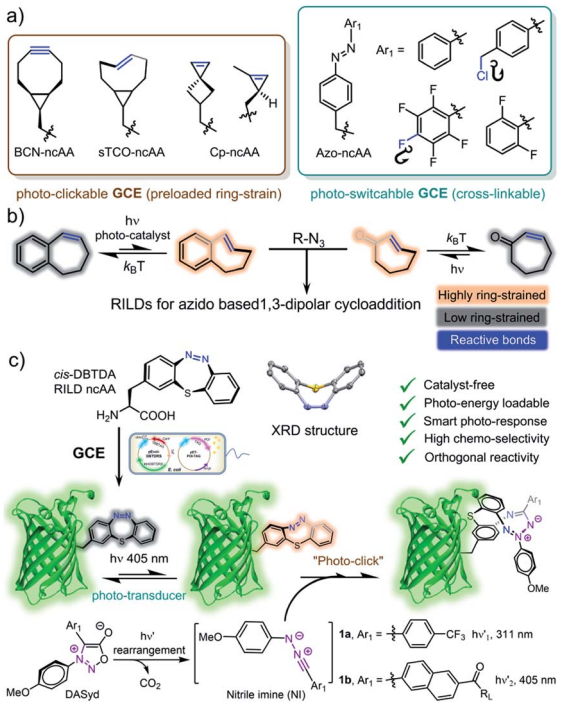

Scheme 1 (a) Conventional photo-clickable and/or photo-switchable ncAAs. (b) Alkene-based RILD photo-click systems. (c) GCE to incorporate the DBTDA on POI site-specifically for integrating RILDs functionality in living contexts.

physical features of exogenous ncAAs at specific residues, the encoded proteins have been exploited for mapping protein–protein interactions (proximity dependent photo-cross-linking),[18] probing and tuning protein structures[19] and the construction of artificial conjugates on demand.[20] In particular, it is of great interest to utilize GCE to encode RILDs (Scheme 1c) because its exceptional biocompatibility and the photochemical energy transduction can enhance the chemoselectivity of the photo-click chemistry.[16] Therefore, the spatiotemporal resolving power of photo-control could be elevated to establish the precise decoration of key residues on proteins of interest (POI) in 3D space to gain high-order functionalization.[21] Inheriting the characteristics of a T-type (another thermal stimulus) photo-switch,[22a] the genetically encoded DBTD residue itself is also well-suited for regulating the microenvironment on a designated site of proteins with fast photoresponse.[22b]

Adding DBTD onto desired residues *via* amber codon suppression could equip the parent proteins with both photoswitch and photo-clickable features (Scheme 1c). To adapt to the hydrophobic pocket of the *Methanosarcina* aminoacyl-tRNA synthetase[17d] with one molecule of adenosine monophosphate (AMP), we designed a compact DBTD–alanine ncAA (DBTDA, Scheme 1c) that is amenable to producing DBTDA tRNA for genetic incorporation. However, there are still two challenges to overcome before realizing spatiotemporally photo-click ligation for visualizing or manipulating biological processes with superior resolution. First, the structure of DBTDA in the thermostable *cis*-configuration resembles a unique "bowl" shaped structure (Scheme 1c), which requires a diversified codon library to evolve the tRNA synthetase to recognize this "exotic" substrate. Second, optimization of the structure of DASyd probes is also essential to achieve high photo-reactivity and chemoselectivity toward DBTD. Through rational design of the codon library in combination with directed evolution toward the *Methanosarcina* tRNA synthetase in the *E. coli* system, we were able to express superfolder green fluorescent proteins (sfGFPs) with the DBTDA incorporated on three individual sites. By encoding the DBTDA into the extracellular domain of the outer membrane porin C protein (OmpC), we also evaluated the efficiency and selectivity of the DASyd-DBTD photo-click reaction on living *E. coli* cells by employing a trifunctional DASyd conjugate. Thus, the distribution of overexpressed OmpC on *E. coli* cells of interest could be captured *in vitro* in 3D space by implementing a designated illumination, which offers a protocol for exploring their dynamic processes in living systems. The successful incorporation of DBTDA also provides a chemical transducer for photochemical energy conversion[23] on key loci of proteins, which could be further exploited in the patterning of proteins in biomaterials[24] and the enrichment of protein molecular machines[25] for synthetic biology,[26] as well as protein photo-pharmaceuticals for precision medicine.[27] The xolographic fabrication of artificial protein copolymers[28] can also be envisioned because DASyd and DBTDA can be photo-activated separately.

Results and discussion

Genetic encoding of DBTDA and identification

In order to obtain a sufficient amount of DBTDA for the directed evolution of the aminoacyl-tRNA synthetase, Smiles rearrangement[29] of diacetyl-thiodiphenylhydrazine (**S3**, Scheme 2) was considered to be a key step to produce the seven-membered cyclic key intermediate, 2-bromo-5,6-diacetyl-5,6-dihydrodibenzo[*b*,*f*][1,4,5]thiadiazepine (**S4**, diacetyl 2*H*-DBTD-Br) in gram scale, which is the precursor for DBTD-Br. After the consecutive deprotection and oxidation of **S4** in air, we were

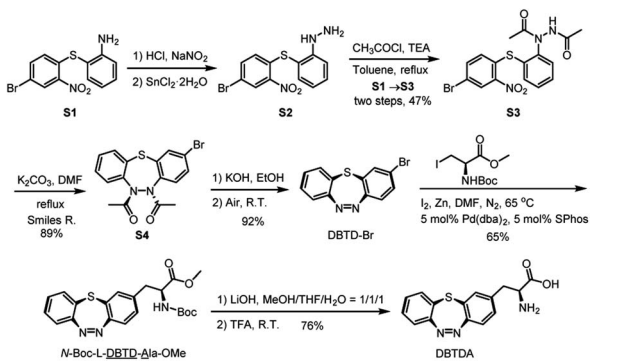

Scheme 2 Synthetic route for L-alanine derived DBTDA ncAA. Pd(dba)$_2$ = bis(dibenzylideneacetone)palladium(0). R.T. = room temperature. R. = rearrangement. SPhos = 2-dicyclohexylphosphino-2′,6′-dimethoxybiphenyl.

able to afford DBTD-Br, and subsequently utilized Negishi coupling[30] with a *N*-Boc-β-iodo-L-alanine-OMe derived organozinc reagent to harvest the desired *N*-Boc-L-DBTD-Ala-OMe, followed by hydrolysis of the ester and deprotection of *N*-Boc to furnish the DBTDA ncAA (Scheme 2).

To genetically encode the DBTDA, we chose the pyrrolysyl-tRNA synthetase/tRNA(PylRS/tRNA) pair from *Methanosarcina* species[31] as the evolving target because of its high efficiency[32] in nonsense codon suppression, flexibility of substrates and full orthogonality in both prokaryotes and eukaryotes (Fig. 1a). It has been proven to be an extraordinary GCE system, and a wide array of ncAAs, *e.g.*, *p*-benzoyl-L-phenyl-alanine (*p*Bpa)[33] and photo-switchable and clickable azobenzene–alanines (Scheme 1a),[34] have been incorporated in both *E. coli* and mammalian cells *via* *Mm*PylRS mutants. However, PylRS variants capable of encoding a seven-membered cyclic azobenzene framework have yet to be developed because of its wide-bodied and bowl-shaped morphology in the *cis*-form. Therefore, we have adopted a rationally designed library from *p*BpaRS mutations[33] to evolve the *Mm*PylRS. The goal of these mutations is to create an appropriate breadthwise space for the rigid and nonplanar macrocyclic DBTD that is orthogonal to other encodable ncAAs. Structural analyses of the *Mm*PylRS binding pocket (PDB code: 2ZIM)[35] for DBTDA clarified the constitution of the library, which includes a series of key residues subjected to either NNK (N = A, T, G or C; K = T or G) site saturation or degenerate-restricted mutagenesis (Tables S1 and S2 ESI†). To our delight, after two rounds of iterative selection of this library with both positive and negative cycles, a distinctive *Mm*PylRS mutant carrying five-residue mutations (Fig. 1b) was obtained in the best consensus, and was named *Mm*DBTDRS, exhibiting the effective incorporation of DBTDA into sfGFP (Fig. 1b). In order to verify the incorporation efficiency and fidelity of *Mm*DBTDRS, we chose three characteristic sites on sfGFP to introduce DBTDA for evaluating its intact expression level. These sites include the N149 and Q204 residues on the outside of the β-barrel, which are in proximity to the sfGFP chromophore and exposed to the solvent,[36] and the K3 site on the *N*-terminus flexible loop.[37] The expression levels of sfGFP-K3DBTD, sfGFP-N149DBTD and sfGFP-Q204DBTD were found to be 2.7, 2.9 and 3.0 mg L^{-1}, respectively, after purification. SDS-PAGE and deconvoluted LC-MS analysis (Fig. 1c) also confirmed the correct molecular weights, in agreement with theoretical predictions (Fig. 1d and S4–S9, ESI†). Furthermore, sfGFP-Q204DBTD was digested by trypsin for LC-MS/MS fingerprinting analysis, which confirmed the fidelity and site-specificity of the *Mm*DBTDRS/tRNA pair, with the successful incorporation of DBTDA into the designated TAG-codon position (Fig. 1e and S1, ESI†). To enhance the incorporation efficiency of DBTDA in *E. coli*, we optimized the concentrations of DBTDA, as well as the pH of the culture medium, during the expression process (Fig. S2, ESI†). Under the optimized conditions (2 mM DBTDA, pH = 8.5), the purified sfGFP-Q204DBTD could be harvested with a yield of 5.7 mg L^{-1}.

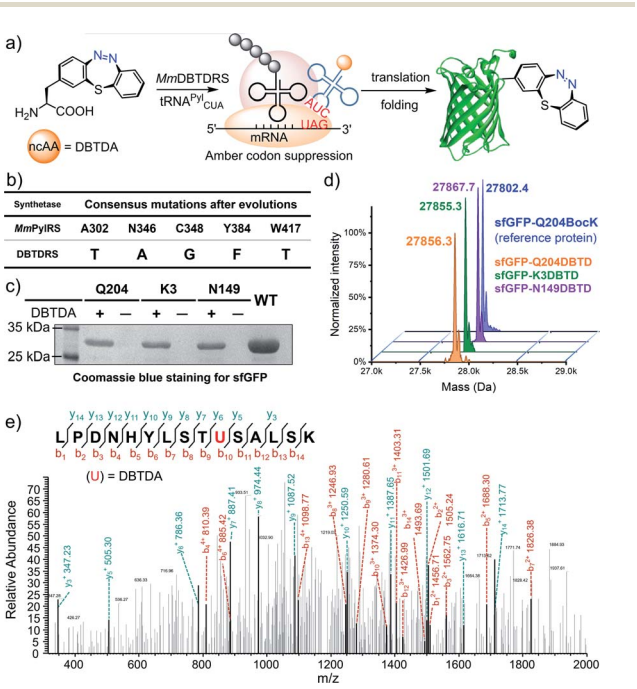

Fig. 1 Genetic incorporation of DBTDA into proteins *via* amber stop-codon suppression. (a) Schematic illustration of the genetic incorporation of DBTDA into designated proteins in living cells. (b) The mutation sites for the construction of the *Mm*PylRS library and the consensus mutant identified as *Mm*DBTDRS after evolution. (c) SDS-PAGE analysis of three purified sfGFPs, sfGFP-K3DBTD, sfGFP-N149DBTD and sfGFP-Q204DBTD, in comparison with the wild-type as a control. (d) Deconvoluted mass spectra for LC-MS analysis of the purified sfGFP-K3DBTD, sfGFP-N149DBTD and sfGFP-Q204DBTD, with sfGFP-Q204BocK shown as the reference. (e) LC-MS/MS analysis of sfGFP-Q204DBTD. The *de novo* sequenced peptide region covering the key 204 residue is displayed and related peptide fragments identified, with the b and y ion peaks marked in the mass-to-charge ratio (*m*/*z*). 204U = 204DBTDA was confirmed to demonstrate the incorporation into sfGFP.

To understand the binding features of DBTDA involved in the protein–substrate interactions for the evolved *Mm*DBTDRS synthetase, we utilized CHARMM-based molecular docking based on the crystal structures of both *Mm*OmeRS (PDB code: 3QTC)[38] and *cis*-DBTD (CCDC code: 1905279).[16a] All of the five residue mutations to the *Mm*PylRS (Fig. 1b) and the putative conformation of L-DBTDA were applied to the active pocket with semi-flexible settings. Therefore, an optimal docking conformation for the *Mm*DBTDRS-DBTDA complex was converged (Fig. 2a) with a binding free energy of −44.2 kcal mol^{-1}. Indeed, DBTDA in the favourable "bowl" shaped energy pose was fitted into the expected binding pocket as the ligand for aminoacylation toward APM. The replacement of W348 and N346 residues with G and A, respectively, reserve a breadthwise space to accommodate the protruding cyclic azobenzene moiety on the DBTDA. The docking simulation also revealed that the DBTDA embeds into a bent binding pocket surrounded by hydrophobic residues, including L305, A346, V401 and I322 (Fig. 2c). As reported previously,[38] T302 is located in the substrate-gating site of *Mm*DBTDRS to form a hydrogen bond (2.9 Å, Fig. 2b) with the α-carboxyl acceptor on the amino acid backbone, stabilizing the polar subunit of DBTDA for acylation. Intriguingly, a lone pair(lp)–π interaction takes place on top of

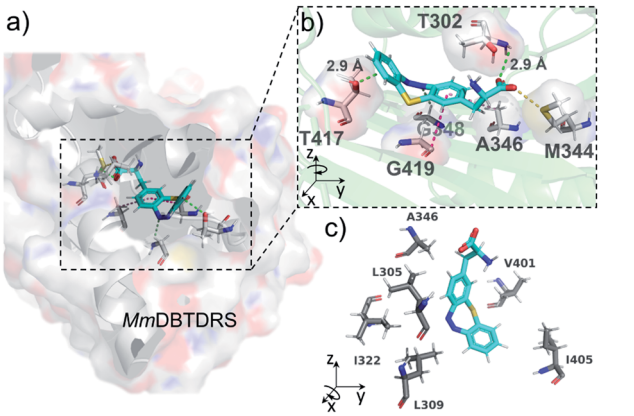

Fig. 2 Molecular docking of DBTDA to the active site of *Mm*DBTDRS. (a) The docking model of DBTDA (cyan) in the *Mm*DBTDRS (gray) complex with side chains of active residues shown in stick form, and viewed from the back. (b) The interactions between DBTDA and amino acid residues in the binding pocket of *Mm*DBTDRS in a magnified front view. T302 (hydrogen bonding, green dotted lines), M344 (sulfur–oxygen interaction, yellow dotted lines), A346 (CH–π interaction, pink dotted lines), G348 (nitrogen–hydrogen bonding, lime dotted lines), G419 (amide–π stacking, magenta dotted lines), T417 (lone pair–π interaction, green dotted lines) and DBTDA (cyan) are highlighted. (c) The hydrophobic interactions between DBTDA (cyan) and L305, L309, I322, A346, V401 and I405 residues (gray).

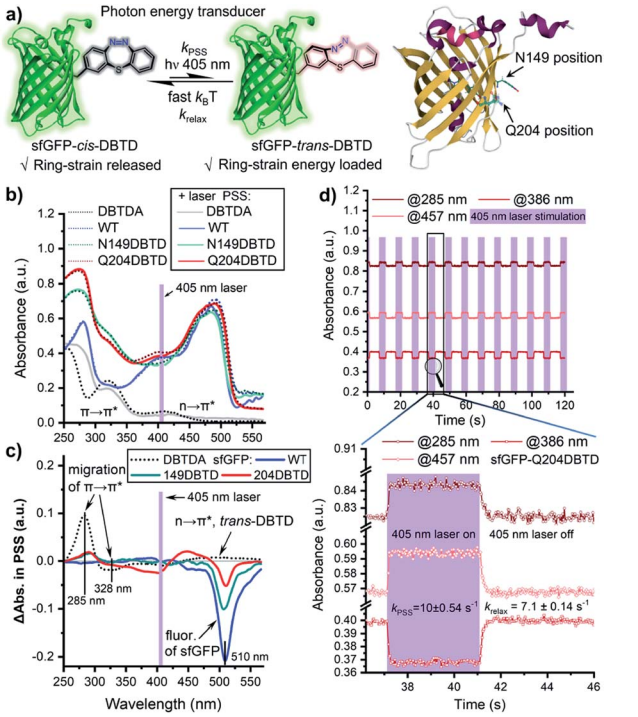

Fig. 3 Photo-switching performance of DBTD residues on the outer surface of sfGFP. (a) Schematic to illustrate the photon-energy transduction of the DBTD residue, and the sites to encode DBTDA. (b) Comparisons of the UV–Vis spectra of both the encoded sfGFP (19.1 μM) and DBTDA (50 μM, 0.1% MeOH) before and after continuous photo-stimulation with a 405 nm laser in PBS (pH = 7.4), 298 K. (c) Variation of the spectra between the PSS and the thermodynamically stable state is shown by displaying the Δabsorbance of the encoded proteins and free DBTDA small molecule. (d) Time-dependent absorbance evolution at three characteristic wavelengths for sfGFP-Q204DBTD. Purple blocks represent the 405 nm laser irradiation pulses. The zoomed-in temporal interval shows the photo-switching kinetics. Laser power density = 250 mW cm^{-2}.

the distal phenyl of DBTDA toward the lone pair electrons of the oxygen atom on the T417 residue (2.9 Å), which might play an important role in keeping the distal phenyl in the right dihedral angle instead of adopting a π–π interaction (Fig. 2b). Compared with another plausible docking posture in which the azo group of DBTDA is flipped and facing outward to the V401 residue in the active pocket (Fig. S3 ESI†), the binding free energy of the displayed posture is advantageous, −44.2 *vs.* −33.3 kcal mol^{-1} (for the latter posture, Fig. S3, ESI†).

Photo-induced ring-strain energy loading of DBTD on proteins

The photo-isomerization performance of a molecular machine might be sensitive to its immediate chemical environment, including the photo-stationary state (PSS) and photo-switching kinetics. These are important factors that have to be considered when GCE is utilized to generate protein mutants for the photo-regulation of functions.[39] To assess the impact of the protein micro-environment on the photo-switching efficiency of DBTD residues, the UV–Vis spectral changes of the two mutants (Q204 and N149) after the DBTD residues were equilibrated to PSS were investigated, using wild-type sfGFP (wt-sfGFP) and free DBTDA as controls (Fig. 3a). Under continuous 405 nm laser photo-stimulation to switch the DBTD residue, the wt-sfGFP did not exhibit any significant absorbance variation in the 250–430 nm region, but a fluorescence peak (510 nm, shown in the Δabsorbance spectra, Fig. 3c) could be observed because the presence of a 405 nm laser also excites the fluorophore of sfGFP simultaneously (Fig. 3b and c). In contrast, free DBTDA showed characteristic π → π* transition changes at both 285 and 328 nm, accompanied by a weak n → π* transition which moved to 450–550 nm under laser irradiation. Intriguingly, mutations of the native amino acid (either Q204 or N149) for DBTDA on sfGFP had an almost identical effect on the absorbance spectral changes around 285 nm (π → π*) after photo-stimulation, in which the PSS was estimated to be higher than 12% for sfGFP-Q204-*trans*-DBTD (Fig. S10, ESI†). But varying degrees of effects from 310 to 550 nm were observed, predominantly on the emission intensity around 510 nm (Fig. 3c). Notably, the Q204DBTD mutant had the most significant effect on the excitation spectral changes from 310–470 nm and there was a sharp suppression of the emission intensity (red line, Fig. 3c), in which the Q204 residue was reported to have a synergistically structural integration with the chromophore of sfGFP.[40] Therefore, sfGFP-Q204DBTD was chosen to study the dynamic response of the photo-switchable DBTD in the protein environment under a programmable photo-stimulation sequence (Fig. 3d). Under an intermittent photo-stimulus, the absorbance signal responded precisely with the input showing no observable decay, outputting a nearly square-signal pattern

at three different wavelengths with distinct phases (for wt-sfGFP as the control, see Fig. S11, ESI†). The ground-state of sfGFP-*cis*-DBTD approaches the PSS with a half-life of 70 ms (k_{PSS}, Fig. 3d) under continuous photo-stimulation, and the energy-loaded "metastable" sfGFP-*trans*-DBTD relaxed back to the ground-state with a half-life of 98 ms (k_{relax}, Fig. 3d) in the dark (lower panel of Fig. 3d and S12, ESI†). Compared with free DBTD ($k_{PSS} = 5.7\ s^{-1}$, $k_{relax} = 3.8\ s^{-1}$),[16] the outer-surface environment at the Q204 position of sfGFP did not hinder the fast photo-response of the DBTD residue to transduce the photon energy into the ring-strain energy, which would accelerate the photo-click ligation for residue-specific labelling.

Selective protein functionalization *via* photo-click chemistry

With the benefits of the DASyd-DBTD photo-click reaction with excellent reactivity and selectivity,[16] we attempted to evaluate the site-specificity of this type of photo-labelling toward the DBTDA encoded sfGFP. Our initial study on the photo-labelling of purified sfGFP–DBTD with DASyd **1a** under irradiation with 311 nm light (capable of the photolysis of **1a**, 10.8 mW cm^{-2}) for 2 min suggested an efficient photo-conjugation, giving the resultant proteins with yields in the order of N149 (85%) > K3 (71%) > Q204 (52%), detected by deconvoluted LC-MS (Fig. S13–S15 ESI†). To visualize this covalent modification *via* in-gel (SDS-PAGE) fluorescence analysis, we utilized **1b-Cy3** (Fig. 4a), a sulfo-Cy3 modified DASyd probe, for *in vitro* protein conjugation on the N149DBTD site to demonstrate the temporal control (Fig. 4b). The SDS-PAGE imaging analysis showed that a Cy3 fluorescence band correlated to sfGFP size was observed for the sample even within 15 s irradiation time *via* a 405 nm LED, and the labelling yield can be controlled in a time-dependent manner. Under optimized conditions, three sfGFP-DBTD mutants after photo-labelling by 3 min irradiation were also subjected to profiling by deconvoluted LC-MS, displaying almost quantitative efficiencies (Fig. 4c and S16–S18, ESI†) with site-specificity (for LC-MS/MS analysis, Fig. S19, ESI†). After subsequent purification to remove small molecules, the molar extinction coefficient (ε) ratio of the fluorophore of sfGFP (485 nm) and the characteristic absorption of the Cy3 (552 nm) can be measured to determine the yield of the labelled protein *via* UV–Vis spectral analysis, which resulted in 94 ± 1.7% yield (Fig. S20 ESI†), consistent with the result from the deconvoluted MS analysis. Through tracking the fluorescent bands in SDS-PAGE, we further analysed the bio-stability of the purified sfGFP–**2b-Cy3** under biologically relevant conditions, *e.g.*, in PBS or in a plasma mimicking environment with 5 mM GSH or even after further 405 nm LED irradiation. The purified sfGFP–**2b-Cy3** was quite stable, without any degradation in PBS (98% retained), and 75% of the intact protein retained in the presence of GSH at 37 °C within 24 hours (Fig. S21 ESI†). Under further 405 nm light exposure for 5 min, 89% and 81% sfGFP–**2b-Cy3** was conserved in PBS and 5 mM GSH, respectively (Fig. S21 ESI†). Even though there was slight protein degradation, the fluorescence of Cy3 remained tagged to the degraded components without being released as free Cy3, indicating that the covalent linkage built by the photo-click reaction is not

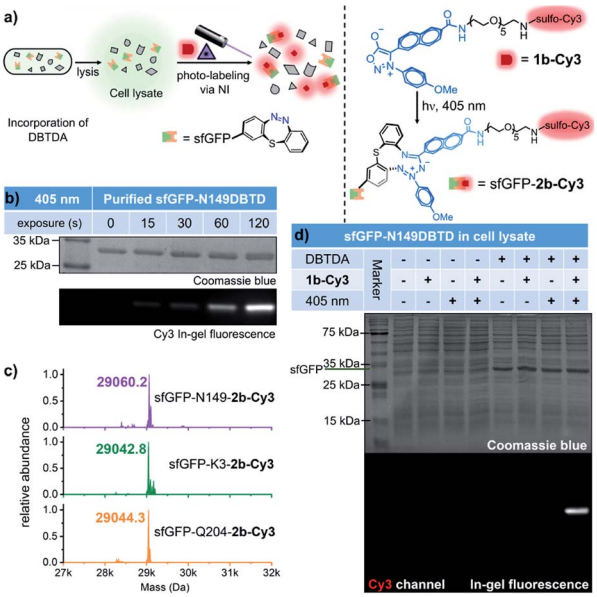

Fig. 4 Temporal controlled and selective modification of sfGFP-DBTD *via* the photo-click reaction with DASyd probes. (a) Schematic work flow for the site-specific photo-labelling of sfGFP-DBTD with the **1b-Cy3** probe. (b) SDS-PAGE imaging analysis for the modification of purified sfGFP-N149DBTD with various irradiation times. Final protein concentration = 5 μM and **1b-Cy3** = 50 μM in PBS (pH = 7.4), a 405 nm LED array (13.4 mW cm^{-2}), 0–120 s. (c) Deconvoluted mass spectra of sfGFP-N149DBTD (purple), sfGFP-K3DBTD (green) and sfGFP-Q204DBTD (orange) after the photo-click reaction with **1b-Cy3**. The final protein concentration = 5 μM and **1b-Cy3** = 250 μM in PBS (pH = 7.4), a 405 nm LED array, 3 min. (d) SDS-PAGE imaging analysis of the labelling of the sfGFP-N149DBTD protein in *E. coli* cell lysate *vs.* a group of control conditions. sfGFP-N149DBTD was over-expressed with 2 mM DBTDA in LB culture medium at pH = 8.5. After cell disruption *via* sonication and centrifugation, 10 μL of the supernatant was diluted with 5 μL of 250 μM **1b-Cy3** in PBS (pH = 7.4) before irradiation with the 405 nm LED array for 3 min.

damaged along with the degradation (Fig. S21 ESI†). These results validated that this photo-click chemistry is an effective tool for photo-controllable ligation toward DBTD-bearing proteins. To expand this photo-chemistry in a live-cell mimicking environment, we treated *E. coli* cell lysates over-expressing sfGFP-N149DBTD with the **1b-Cy3** probe, and implemented the ligation under the optimized conditions, followed by resolving *via* SDS-PAGE (Fig. 4d). Gratifyingly, only cell lysate containing the DBTD reporter on sfGFP exhibited an exclusive and strong fluorescent band after 405 nm illumination, which also matched the size of sfGFP. In contrast, there was rarely any fluorescent band detected in lanes for the samples either without DBTD on the proteins or under control conditions. Coomassie blue staining confirmed the fluorescence signal overlapping with the over-expressed sfGFP band (Fig. 4d). The photo-labelling experiments in cell lysate revealed the excellent selectivity of the DASyd-DBTD photo-click chemistry, capable of targeting the DBTD residues on a specific site in a complex of proteins.

Since sfGFP-DBTD could be over-expressed in the living BL21(DE3) strain, we also attempted to evaluate intracellular

bioorthogonal conjugation by utilizing a live-cell permeable probe, **DASyd-Fl** (photolysis under 373 nm LED, 38.5 mW cm^{-2}) toward DBTDA residues under the excitation of both 373 nm and 405 nm LED (Fig. S22 ESI†). After the photo-click procedure inside living cells, SDS-PAGE analysis of the cell lysate revealed the successful labelling of the sfGFP-DBTD as a fluorescence band with the right size was detected. However, there were other stronger bands detected in the gel at the same time, which were likely attributed to the undesired binding of the **DASyd-Fl** dye to native proteins or to lipid phase components in the living *E. coli* cells. Therefore, the decent bioorthogonality of the DASyd-DBTD photo-click system with the anionic **1b-Cy3** probe is more suitable for us to study the dynamics of proteins in a single living cell when a spatiotemporal irradiation of submicron resolution could be exerted.

Spatiotemporally controlled and selective fluorescence labelling of the DBTDA encoded proteins on *E. coli* cells

OmpC, known as a member of the outer membrane proteins (OMPs) family in Gram-negative bacteria, serves as a passive diffusion porin for transporting small molecules in the homotrimer form,[41] and its expression level is regulated by external osmolarity.[42] As a pharmacological target against antibiotic resistance,[43] whether OmpC participates in the transport of other essential small molecules to support bacterial survival, as well as its dynamic distribution on cells, is yet to be discovered.

Encouraged by the specific labelling of DBTD-bearing sfGFP, we were able to exploit the advantages of the DASyd-DBTD photo-click chemistry in the functionalization of OmpC-Y232DBTD[44] on living *E. coli* cells under photo-control with high precision (Fig. 5a). The Y232 mutation site was chosen according to previous studies[45] in which its location on one of the eight external loops of OmpC was pointed out. Live BL21(DE3) cells over-expressing either intact OmpC-Y232DBTD (2 mM DBTDA) or truncated OmpC (without DBTDA) *via* transformation with both pET-OmpC-Y232TAG and pEvol-*Mm*DBTDRS were subjected to photo-click ligation with the **1b-Cy3** conjugate *via* exposure to the 405 nm LED for 5 min in PBS. The decorated cells were subsequently lysed, and the lysates were resolved by an in-gel fluorescence assay to investigate the selectivity of the photo-conjugation (Fig. S23 ESI†). To our delight, we could observe a prominent Cy3 fluorescence band of the correct OmpC size only in the lane where the prerequisites for the photo-click reaction were met, rather than those lanes under control conditions, indicating that the excellent chemoselectivity of the photo-click chemistry is broadly applicable.

For the purpose of immunofluorescence labelling, we also constructed a biotinylated DASyd probe, **1b-Cy3-Biotin** (Fig. 5b), which integrates three functionalities and displays photoreactivity akin to **1b-Cy3**. Therefore, multi-colored fluorescence Western blot (WB) imaging was performed to verify the chemical selectivity of the photo-click chemistry by staining the lysate PVDF membrane with the NeutrAvidin™-OG-488 probe for recognizing the photo-ligated biotin motif on OmpC (Fig. 5c). Encouragingly, the exclusive and overlapped bands shown in both the Cy3 channel and OG-488 channel reflected that the photo-conjugation was specifically targeted to the desired OmpC-Y232DBTD in the context of living cells.

After immobilization in agarose gels for the purpose of imaging, only intact BL21(DE3) cells over-expressing OmpC-Y232DBTD showed strong Cy3 fluorescence on the outer membrane,[46] which was clarified by laser scanning confocal microscopic imaging (59% of the total cells were strongly labelled, Fig. 5d). Cells expressing truncated OmpC cannot be photo-labelled. Intriguingly, although most of the photo-labelled bacterial cells showed a uniform outer membrane fluorescence morphology, individual cells exhibited unique distributions of OmpC in either bipolar or multi-spotted shapes on the surface of cells (white arrows, Fig. 5d), which suggests the potential aggregation of the intact OmpC. Notably, inclusion bodies could be imaged when truncated OmpC was accumulated inside the *E. coli* cells either with very poor amber stop codon suppression efficiency (Fig. 5d upper row, blue arrows) or in the absence of DBTDA (Fig. 5d lower row, blue arrows).[46]

To demonstrate the spatial resolving power of the DASyd-DBTD photo-click chemistry, we projected a localized illumination in a rectangular shape (307 μm × 176 μm) *via* an embedded digital micromirror device (DMD) in the microscopic system to the cells over-expressing OmpC-Y232DBTD after treatment with **1b-Cy3-Biotin** (Fig. 5e). The resulting images indicated that most of the *E. coli* cells inside the exposed area emitted the Cy3 fluorescence signal, whereas cells outside the area scarcely showed any signals. A few cells outside the stimulated area but close to the boundary were also photo-labelled, but the fluorescence intensity was relatively weak (Fig. 5e, green arrows). These results suggested that the genetically encoded DBTDA could potentially be utilized to unravel the functionalities of OmpC on single cells by more sophisticated irradiation in regions of interest (ROI). Thus, we projected a grid-patterned photo-stimulation *via* the DMD (405 nm LED, minimal grid line width = 0.44 μm) onto a cluster of *E. coli* cells over-expressing OmpC-Y232DBTD after treatment with 5 μM **1b-Cy3-Biotin** (Fig. 5f) to preliminarily assess the spatial resolution. Encouragingly, the fluorescently labeled cells were mainly located within the grid lines of the stimulation pattern, although there was some offset labelling, presumably caused by either light scattering (the focal plane of the 100× objective is very thin) or diffusion of the photo-generated NI intermediate. Due to the varying expression level of GCE in encoding the DBTDA,[47] about 40% of the total cells on the grid lines were strongly photo-labelled (Fig. 5f). We also found "U-shaped" subcellular fluorescence signals (Fig. 5f, yellow arrows) corresponding to half-segments of the bacterial outer membrane, which suggest that the spatial resolution of this photo-stimulation, together with the photo-click system, could be higher than the size of an *E. coli* cell (length < 3 μm, width ≈ 1 μm).[48]

To better characterize the distribution of OmpC on *E. coli* cell *via* photo-click chemistry in 3D space, we projected the same grid-patterned photo-stimulation (*via* the DMD, 405 nm LED) onto clusters of cells over-expressing OmpC-Y232DBTD after treatment with 5 μM **1b-Cy3-Biotin** (Fig. 6a, for other groups of imaging results as replications, see S24 and S25, ESI†). After washing, an 18-slice fluorescence tomogram covering the region

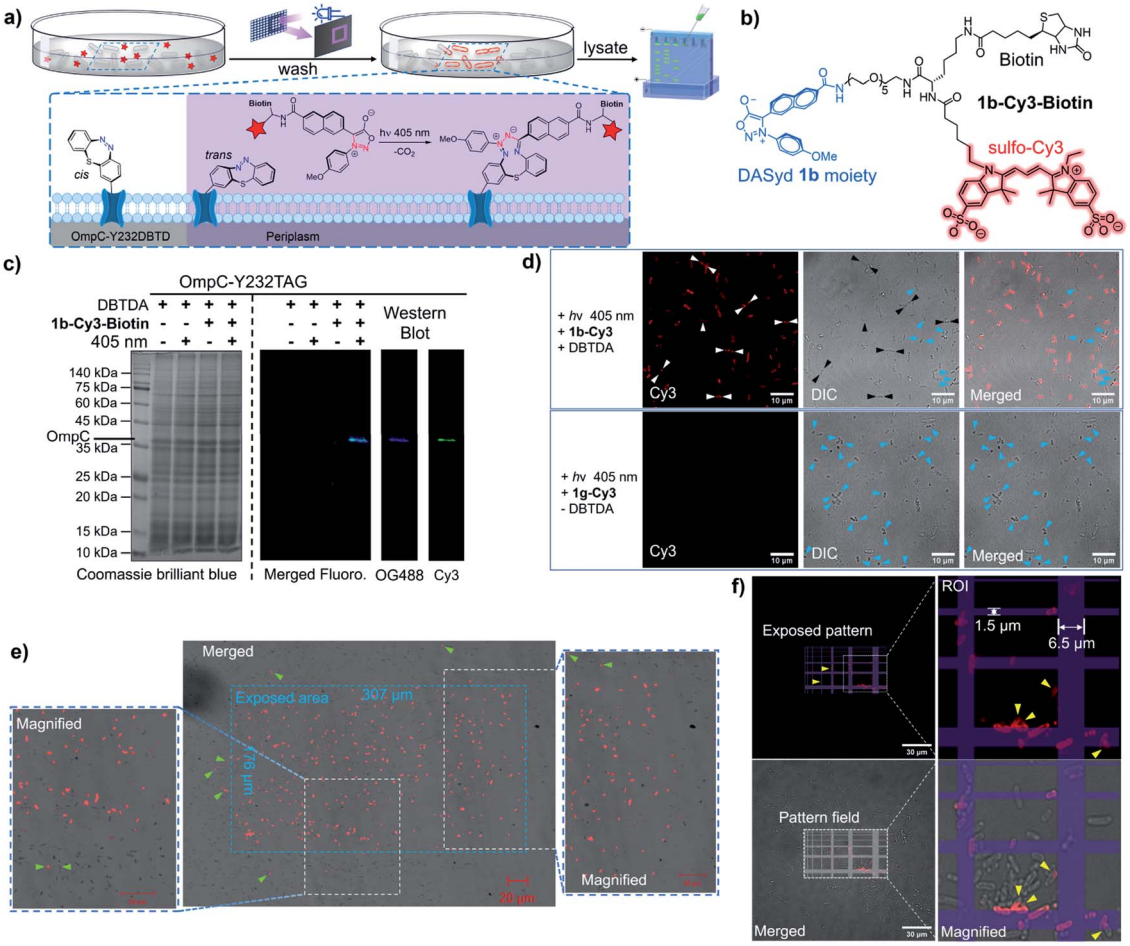

Fig. 5 Spatiotemporally resolved fluorescence labelling of living *E. coli* cells. (a) Schematic view of the model for the labelling of OmpC-DBTD on the outer membrane of *E. coli* cells *versus* regions outside the irradiation area. (b) Chemical structure of the DASyd fluorescent probe, **1b-Cy3-Biotin**. (c) Dual-colour fluorescence Western blot analysis of the photo-click labelled OmpC-Y232DBTD in *E. coli* cell lysates using the NeutrAvidin™ Oregon Green™ 488 conjugate as the antibody. (d) Fluorescence confocal microscopic imaging showing specific labelling of OmpC on *E. coli* cells. Conditions: 25 μM **1b-Cy3** in PBS (pH = 7.4), 298 K, 405 nm LED array (13.4 mW cm^{-2}), 5 min. *E. coli* cells displaying labelling on the poles of the rod shape or as scattered spots were pinpointed by white arrows in the Cy3 channel and black arrows in differential interference contrast (DIC) channel (upper row). The *E. coli* cells containing the inclusion bodies are denoted by blue arrows in the DIC and merged channels (lower row). (e) Spatial control of the fluorescence labelling of OmpC-Y232TAG on the outer membrane surface of *E. coli* cells within a designated irradiation block of 405 nm LED, projected through an embedded DMD in the fluorescence microscope. Conditions: 5 μM **1b-Cy3-Biotin** in PBS (pH = 7.4), 298 K, 405 nm LED, 5 s. The *E. coli* cells labelled outside the irradiation area are denoted by green arrows; image acquisition: excitation = 543 nm, emission = 615 nm. (f) Spatial control under a patterned irradiation of 405 nm LED projected through an embedded DMD for 30 s. The *E. coli* cells displaying partial membrane fluorescence labelling are denoted by yellow arrows. Scale bar = 10 or 20 or 30 μm.

of the photo-stimulated cells was acquired with a Z-stepping of 0.20 μm and reconstructed into a 3D Z-stacking model (Fig. 6b). The volumetric rendering allowed us to understand in more detail the distribution of OmpC on the outer membrane. As a result, the pattern of Cy3 fluorescence on *E. coli* cells was mostly overlapped with the photo-stimulation pattern in 3D space (Fig. 6b and c). Although, the scattering of light (multi-layer structure of bacterial clusters) and diffusion of the NI intermediate resulted in some diffused fluorescence labelling at the edges of the stimulated area, depending on the Z-axial position and expression level of OmpC-DBTD of individual cells (Fig. 6d, f and S24, ESI†). It is noteworthy that subcellular segments on specific *E. coli* cells could be precisely distinguished at the edge of the photo-illumination lines, which were highlighted in the magnified 3D scene (yellow arrows, Fig. 6c). Furthermore, the cross-section slices in both the transverse and longitudinal direction also supported that the labelled OmpC is localized on the outer membrane because the typical hollow ring-shape of the Cy3 signal could be observed (Fig. 6d). In fact, Z-sliced images picked from the tomogram revealed that some of the Cy3 fluorescence signals distributed granularly on the outer membrane, presumably due to aggregation of the over-expressed OmpC (Fig. 6d and f), especially for few filamented cells (Fig. S25, ESI†).[49] We also noticed that some of *E. coli* cells displayed enriched OmpC at both poles of the rod shape (white arrows, Fig. 6d and S24d, ESI†). In particular, some

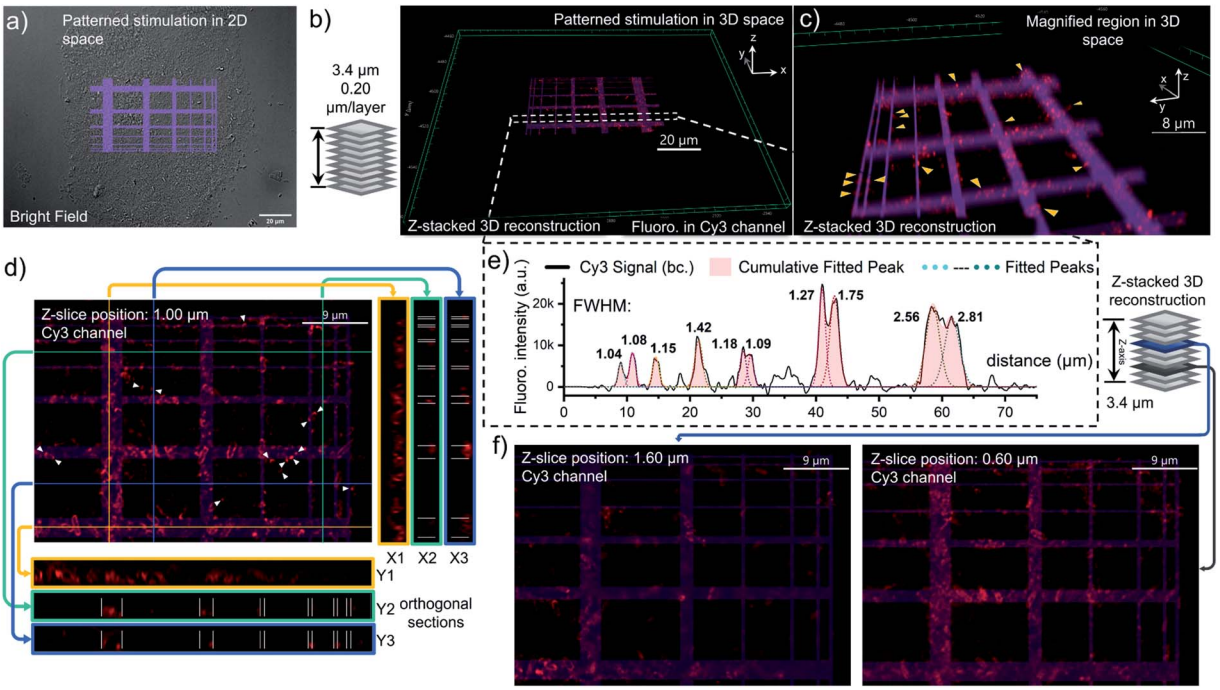

Fig. 6 Photo-click labelling of the OmpC porin on *E. coli* cells with enhanced spatiotemporal control, and the Cy3 fluorescence distribution analysis for the labelled OmpC in 3D space. (a) DIC image of *E. coli* cells with a grid pattern of 405 nm photo-stimulation shown in 2D space. (b) 3D reconstruction displaying the Cy3-labelled *E. coli* cells overlapping within the photo-stimulation pattern. Z-stacking of 18-slice tomograms. Interval of each layer = 0.20 μm, full thickness in *Z*-axis = 3.40 μm. Experimental conditions: 5 μM **1b-Cy3-Biotin**, 405 nm, 30 s, then washed with PBS three times before imaging. (c) Magnified region of interest in the rendered 3D space to show the fluorescence labelling at the subcellular level. Yellow arrows pinpoint the featured cells with partial fluorescence labelling on the outer membrane. (d) Diagram to show cross-sectional images at three different *X*–*Z* and *Y*–*Z* coordinate planes to display the labelled *E. coli* cells on different *Z*-axis cross-sections of the photo-stimulation pattern. Z-slice position: 1.00 μm. (e) Quantification of the spatiotemporal resolution of the photo-click between OmpC-Y232DBTD and **1b-Cy3-Biotin**. Plot of the mean fluorescence intensity profile (black colored curve, bc. = baseline corrected) along the white dotted strip in the Cy3 channel of (b) with the FWHM (in μm) of each peak displayed. The square signals were fitted with Gaussian distributions (dotted lines) to obtain the FWHM on both edges. The seven main signal peaks (pink filled) represent the fluorescence labelling results across the seven grid lines with increasing widths, along with the photo-stimulus pattern. (f) Other Z-slice images with magnified regions showing the overlapping between photo-stimulated grid lines and the Cy3 fluorescence signal, also focusing on the possible diffusion of the Cy3 signal on *E. coli* cells. Z-slice positions: 1.60 and 0.60 μm.

of them even appeared in pairs with a pole-to-pole spliced form. Therefore, it is possible that the pole distribution of OmpC might be related to the division of the bacterial cell (enlarged image in Fig. S24e, ESI†).[50] Nevertheless, it is evident that there was some off-site and diffused Cy3 labelling shown in the imprinted fluorescence pattern (Fig. 6d and f). In addition, the spatial resolution of this photo-click approach on *E. coli* cells was assessed by the full width at half maximum (FWHM) of the imprinted Cy3 signal peak across the photo-stimulation line, which was determined to be as low as 1.1 μm on average (Fig. 6e). Considering that readily available LEDs were used as the light sources and DMD & epi-fluorescence microscopy were utilized as the photo-stimulation and imaging platform, respectively, the spatial resolution of 1.1 microns is decent.

Subsequently, we further employed an excitation pattern of a dot array *via* the DMD to evaluate the spatial-resolution of the photo-click labelling on OmpC at the single-cell level. The dot array was programmed to contain single-pixel excitations (the irradiation spot is roughly 135 nm per pixel on the specimen, Fig. S26, ESI†) to possibly demonstrate the finest resolution of the current photo-stimulation system. Surprisingly, the photo-stimulation of single-pixel dots could selectively label individual cells (Fig. S26, ESI†) in designated clusters of *E. coli* cells, albeit with some background labelling. Further study using laser (even femtosecond laser) scanning technology for stimulation and imaging is underway for a higher spatial resolution.

To be able to further track the dynamics of the photo-labelled OmpC on living cells, we also compared the survival of the BL21 strain before and after the photo-click reaction. The colony counting suggested that the photo-labelling of the over-expressed OmpC-DBTD protein on the outer membrane would cause a significantly weakened viability (10% survival rate, Fig. S27 ESI†). Meanwhile, applying the photo-stimulation (405 nm) alone would not lead to a bactericidal effect (78% survival rate, slight phototoxicity). As a result, the introduction of larger-sized dye conjugates on the outer membrane domain (Y232) of OmpC might alter the porin nature of OmpC into an accumulated hybrid conjugate that is possibly interfering with essential cellular processes.[46] These data collectively suggested that the genetic incorporation of DBTDA in combination with the DASyd-DBTD photo-click chemistry enables spatiotemporal OmpC decoration on living cell membranes, offering the

potential of triggering protein-mediated bactericidal activity selectively under photo-control. However, the incorporation sites of DBTDA can be expanded and screened to diversify the photo-functionalization of target proteins in living systems.

Conclusions

We have developed a novel ncAA bearing DBTD motif as a photo-switchable RILD reporter, and also evolved an *Mm*DBTDRS/$tRNA_{CUA}$ pair to allow its GCE incorporation into recombinant proteins site-specifically in *E. coli* systems. The incorporation efficiency of DBTDA into proteins was optimized and the binding model of DBTDA to the evolved synthetase was clarified by molecular docking to shed light on the design of synthase evolution for the incorporation of DBTDA derivatives. The successful incorporation of DBTDA facilitates the exploration of the photo-transducing performance of the DBTD residue on proteins, and also the photo-click conjugation between DBTD-encoded proteins and fluorescent DASyd probes in living cells with an excellent reaction rate, chemoselectivity and site-specificity. Moreover, an outer membrane porin C protein on *E. coli* cells was chosen to unravel its features and distribution characteristics *via* photo-click labelling in harmony with the genetically encoded DBTDA on its extracellular domain. By employing the DBTD as a RILD reporter together with the photo-generated nitrile imine, the spatial decoration of OmpC is now approaching the single-cell level. Encoding the DBTD reporter with both fast photo-response and photo-click features on proteins in a site-specific manner holds great potential for developing high-order manipulation of functionalized proteins *via* photon energy transduction in widespread application scenarios.

Data availability

Additional figures as described in the main text, all experimental procedures, synthetic procedures, and copies of spectral data of the compounds and processes, computational details are available in the ESI.†

Author contributions

Qin Xiong performed most of the experimental work in this manuscript and drafted the manuscript. Tingting Zheng assisted in the synthesis of chemical reagents and also in protein expression, purification and characterization. Xin Shen assisted in the photo-switching experiments. Baolin Li synthesized DASyd **1a** and **1b**. Jielin Fu performed the construction of pET-sfGFP-XTAG plasmids. Xiaohu Zhao participated in the analysis of ^{1}H and ^{13}C NMR spectra. Chunxia Wang revised the manuscript. Zhipeng Yu synthesized the fluorescent probe **1b-Cy3-Biotin**, conceived of the project, analyzed the data and wrote the manuscript.

Conflicts of interest

There are no conflicts to declare.

Acknowledgements

We thank Yanhong Liu at the Comprehensive Training Platform of Specialized Laboratory, College of Chemistry, for her assistance with the confocal image collection. We are grateful to Dr Pengchi Deng at the Analytical & Testing Center, SCU for help with NMR spectrum acquisition for the PSS. Financial support was provided by the National Natural Science Foundation of China (22001181 and 22077090) and the Fundamental Research Funds for the Central Universities (20826041D4117) and Institutional Research Fund from Sichuan University (2020SCUNL105). We also thank Dr Wenshe Liu (Texas A&M) and Dr Qing Lin (SUNY-UB) for generously providing us the plasmids, pEvol-PylT-PylRS and pET-sfGFP-Q204TAG. We also appreciate Dr Lunzhi Dai (State Key Laboratory of Biotherapy and Cancer Center, West China Hospital, Sichuan University) for help with the LC-MS/MS analysis.

Notes and references

1 (*a*) H. C. Kolb, M. G. Finn and K. B. Sharpless, *Angew. Chem., Int. Ed.*, 2001, **40**, 2004; (*b*) C. R. Becer, R. Hoogenboom and U. S. Schubert, *Angew. Chem., Int. Ed.*, 2009, **48**, 4900.
2 P. Thirumurugan, D. Matosiuk and K. Jozwiak, *Chem. Rev.*, 2013, **113**, 4905.
3 W. Xi, T. F. Scott, C. J. Kloxin and C. N. Bowman, *Adv. Funct. Mater.*, 2014, **24**, 2572.
4 (*a*) H. Wang, M. Gauthier, J. R. Kelly, R. J. Miller, M. Xu, W. D. O'Brien Jr and J. Cheng, *Angew. Chem., Int. Ed.*, 2016, **55**, 5452; (*b*) K. Lang, L. Davis, J. Torres-Kolbus, C. Chou, A. Deiters and J. W. Chin, *Nat. Chem.*, 2012, **4**, 298.
5 M. A. Tasdelen and Y. Yagci, *Angew. Chem., Int. Ed.*, 2013, **52**, 5930.
6 B. D. Fairbanks, L. J. Macdougall, S. Mavila, J. Sinha, B. E. Kirkpatrick, K. S. Anseth and C. N. Bowman, *Chem. Rev.*, 2021, **121**, 6915.
7 (*a*) C. E. Hoyle and C. N. Bowman, *Angew. Chem., Int. Ed.*, 2010, **49**, 1540; (*b*) S. Chatani, C. J. Kloxin and C. N. Bowman, *Polym. Chem.*, 2014, **5**, 2187.
8 (*a*) R. A. Olson, A. B. Korpusik and B. S. Sumerlin, *Chem. Sci.*, 2020, **11**, 5142; (*b*) N. A. Repina, T. McClave, H. J. Johnson, X. Bao, R. S. Kane and D. V. Schaffer, *Cell Rep.*, 2020, **31**, 107737.
9 G. S. Kumar and Q. Lin, *Chem. Rev.*, 2021, **121**, 6991.
10 (*a*) Y. Wang, W. Song, W. J. Hu and Q. Lin, *Angew. Chem., Int. Ed.*, 2009, **48**, 5330; (*b*) Z. Yu, T. Y. Ohulchanskyy, P. An, P. N. Prasad and Q. Lin, *J. Am. Chem. Soc.*, 2013, **135**, 16766; (*c*) Y. Wu, G. Guo, J. Zheng, D. Xing and T. Zhang, *ACS Sens.*, 2019, **4**, 44; (*d*) S. Jiang, X. Wu, H. Liu, J. Deng, X. Zhang, Z. Yao, Y. Zheng, B. Li and Z. Yu, *ChemPhotoChem*, 2020, **4**, 327.
11 (*a*) L. Zhang, X. Zhang, Z. Yao, S. Jiang, J. Deng, B. Li and Z. Yu, *J. Am. Chem. Soc.*, 2018, **140**, 7390; (*b*) X. Zhang, X. Wu, S. Jiang, J. Gao, Z. Yao, J. Deng, L. Zhang and Z. Yu, *Chem. Commun.*, 2019, **55**, 7187.
12 (*a*) S. Arumugam and V. V. Popik, *J. Am. Chem. Soc.*, 2011, **133**, 5573; (*b*) S. Arumugam, S. V. Orski, J. Locklin and V. V. Popik, *J. Am. Chem. Soc.*, 2012, **134**, 179.

13 A. A. Poloukhtine, N. E. Mbua, M. A. Wolfert, G.-J. Boons and V. V. Popik, *J. Am. Chem. Soc.*, 2009, **131**, 15769.
14 (*a*) J. Wang, W. Zhang, W. Song, Y. Wang, Z. Yu, J. Li, M. Wu, L. Wang, J. Zang and Q. Lin, *J. Am. Chem. Soc.*, 2010, **132**, 14812; (*b*) Y. Tian, M. P. Jacinto, Y. Zeng, Z. Yu, J. Qu, W. R. Liu and Q. Lin, *J. Am. Chem. Soc.*, 2017, **139**, 6078; (*c*) Z. Yu, Y. Pan, Z. Wang, J. Wang and Q. Lin, *Angew. Chem., Int. Ed.*, 2012, **51**, 10600; (*d*) Y. Wang, W. Song, W. J. Hu and Q. Lin, *Angew. Chem., Int. Ed.*, 2009, **48**, 5330; (*e*) Z. Yu and Q. Lin, *J. Am. Chem. Soc.*, 2014, **136**, 4153.
15 (*a*) K. Singh, C. J. Fennell, E. A. Coutsias, R. Latifi, S. Hartson and J. D. Weaver, *Chem*, 2018, **4**, 124; (*b*) H. Yang, T. Zeng, S. Xi, S. Hu, Y. Wu and Y. Tang, *Green Chem.*, 2020, **22**, 7023.
16 (*a*) J. Gao, Q. Xiong, X. Wu, J. Deng, X. Zhang, X. Zhao, P. Deng and Z. Yu, *Commun. Chem.*, 2020, **3**, 29; (*b*) J. Deng, X. Wu, G. Guo, X. Zhao and Z. Yu, *Org. Biomol. Chem.*, 2020, **18**, 5602.
17 (*a*) L. Davis and J. W. Chin, *Nat. Rev. Mol. Cell Biol.*, 2012, **13**, 168; (*b*) A. Dumas, L. Lercher, C. D. Spicer and B. G. Davis, *Chem. Sci.*, 2015, **6**, 50; (*c*) J. W. Chin, *Nature*, 2017, **550**, 53; (*d*) J. M. Kavran, S. Gundllapalli, P. O'Donoghue, M. Englert, D. Söll and T. A. Steitz, *Proc. Natl. Acad. Sci. U. S. A.*, 2007, **104**, 11268.
18 (*a*) T.-A. Nguyen, M. Cigler and K. Lang, *Angew. Chem., Int. Ed.*, 2018, **57**, 14350; (*b*) W. Hu, Y. Yuan, C.-H. Wang, H.-T. Tian, A.-D. Guo, H.-J. Nie, H. Hu, M. Tan, Z. Tang and X.-H. Chen, *Chem*, 2019, **5**, 2955; (*c*) H. Mori and K. Ito, *Proc. Natl. Acad. Sci. U. S. A.*, 2006, **103**, 16159.
19 (*a*) J. C. Jackson, J. T. Hammill and R. A. Mehl, *J. Am. Chem. Soc.*, 2007, **129**, 1160; (*b*) S. E. Cellitti, D. H. Jones, L. Lagpacan, X. Hao, Q. Zhang, H. Hu, S. M. Brittain, A. Brinker, J. Caldwell, B. Bursulaya, G. Spraggon, A. Brock, Y. Ryu, T. Uno, P. G. Schultz and B. H. Geierstanger, *J. Am. Chem. Soc.*, 2008, **130**, 9268; (*c*) L. Wang, J. Zhang, M.-J. Han, L. Zhang, C. Chen, A. Huang, R. Xie, G. Wang, J. Zhu, Y. Wang, X. Liu, W. Zhuang, Y. Li and J. Wang, *Angew. Chem., Int. Ed.*, 2021, **60**, 11143.
20 (*a*) J. H. Mills, S. D. Khare, J. M. Bolduc, F. Forouhar, V. K. Mulligan, S. Lew, J. Seetharaman, L. Tong, B. L. Stoddard and D. Baker, *J. Am. Chem. Soc.*, 2013, **135**, 13393; (*b*) Y. Fu, J. Huang, Y. Wu, X. Liu, F. Zhong and J. Wang, *J. Am. Chem. Soc.*, 2021, **143**, 617; (*c*) J. Wang, Y. Liu, Y. Liu, S. Zheng, X. Wang, J. Zhao, F. Yang, G. Zhang, C. Wang and P. R. Chen, *Nature*, 2019, **569**, 509.
21 (*a*) V. Klippenstein, L. Mony and P. Paoletti, *Trends Biochem. Sci.*, 2018, **43**, 436; (*b*) J.-Y. Kang, D. Kawaguchi, I. Coin, Z. Xiang, D. D. M. O'Leary, P. A. Slesinger and L. Wang, *Neuron*, 2013, **80**, 358; (*c*) S. Liu, C. Lin, Y. Xu, H. Luo, L. Peng, X. Zeng, H. Zheng, P. R. Chen and P. Zou, *Nat. Chem.*, 2021, **13**, 472.
22 (*a*) S. Crespi, N. A. Simeth, M. D. Donato, S. Doria, C. N. Stindt, M. F. Hilbers, F. L. Kiss, R. Toyoda, S. Wesseling, W. J. Buma, B. L. Feringa and W. Szymański, *Angew. Chem., Int. Ed.*, 2021, **60**, 25290; (*b*) M. Bose, D. Groff, J. Xie, E. Brustad and P. G. Schultz, *J. Am. Chem. Soc.*, 2006, **128**, 388.
23 Q.-Q. Zhou, Y.-Q. Zou, L.-Q. Lu and W.-J. Xiao, *Angew. Chem., Int. Ed.*, 2019, **58**, 1586.
24 (*a*) C. Guo, H. Kim, E. M. Ovadia, C. M. Mourafetis, M. Yang, W. Chen and A. M. Kloxin, *Acta Biomater.*, 2017, **56**, 80; (*b*) M. A. Wijdeven, C. Nicosia, A. Borrmann, J. Huskens and F. L. van Delft, *RSC Adv.*, 2014, **4**, 10549; (*c*) A. D. de Araújo, J. M. Palomo, J. Cramer, M. Köhn, H. Schröder, R. Wacker, C. Niemeyer, K. Alexandrov and H. Waldmann, *Angew. Chem., Int. Ed.*, 2006, **45**, 296.
25 A. M. Hartley, H. L. Worthy, S. C. Reddington, P. J. Rizkallah and D. D. Jones, *Chem. Sci.*, 2016, **7**, 6484.
26 Y. Wang, X. Chen, W. Cai, L. Tan, Y. Yu, B. Han, Y. Li, Y. Xie, Y. Su, X. Luo and T. Liu, *Angew. Chem., Int. Ed.*, 2021, **60**, 10040.
27 X. Ji, Z. Pan, B. Yu, L. K. De La Cruz, Y. Zheng, B. Ke and B. Wang, *Chem. Soc. Rev.*, 2019, **48**, 1077.
28 M. Regehly, Y. Garmshausen, M. Reuter, N. F. König, E. Israel, D. P. Kelly, C.-Y. Chou, K. Koch, B. Asfari and S. Hecht, *Nature*, 2020, **588**, 620.
29 (*a*) A. A. Levy, H. C. Rains and S. Smiles, *J. Chem. Soc.*, 1931, 3264; (*b*) C. Corral, J. Lissavetzky and G. Quintanilla, *J. Org. Chem.*, 1982, **47**, 2214.
30 Z. Yao, X. Wu, X. Zhang, Q. Xiong, S. Jiang and Z. Yu, *Org. Biomol. Chem.*, 2019, **17**, 6777.
31 (*a*) G. Srinivasan, C. M. James and J. A. Krzycki, *Science*, 2002, **296**, 1459; (*b*) S. M. Hancock, R. Uprety, A. Deiters and J. W. Chin, *J. Am. Chem. Soc.*, 2010, **132**, 14819; (*c*) P. R. Chen, D. Groff, J. Guo, W. Ou, S. Cellitti, B. H. Geierstanger and P. G. Schultz, *Angew. Chem., Int. Ed.*, 2009, **48**, 4052; (*d*) S. Greiss and J. W. Chin, *J. Am. Chem. Soc.*, 2011, **133**, 14196; (*e*) A. Bianco, F. M. Townsley, S. Greiss, K. Lang and J. W. Chin, *Nat. Chem. Biol.*, 2012, **8**, 748.
32 M. Pott, M. J. Schmidt and D. Summerer, *ACS Chem. Biol.*, 2014, **9**, 2815.
33 V. K. Lacey, G. V. Louie, J. P. Noel and L. Wang, *ChemBioChem*, 2013, **14**, 2100.
34 (*a*) C. Hoppmann, V. K. Lacey, G. V. Louie, J. Wei, J. P. Noel and L. Wang, *Angew. Chem., Int. Ed.*, 2014, **53**, 3932; (*b*) C. Hoppmann, I. Maslennikov, S. Choe and L. Wang, *J. Am. Chem. Soc.*, 2015, **137**, 11218.
35 J. M. Kavran, S. Gundllapalli, P. Donoghue, M. Englert, D. Söll and T. A. Steitz, *Proc. Natl. Acad. Sci. U. S. A.*, 2007, **104**, 11268.
36 (*a*) S. C. Reddington, E. M. Tippmann and D. Dafydd Jones, *Chem. Commun.*, 2012, **48**, 8419; (*b*) T. M. Roberts, F. Rudolf, A. Meyer, R. Pellaux, E. Whitehead, S. Panke and M. Held, *Sci. Rep.*, 2016, **6**, 28166.
37 J.-D. Pédelacq, S. Cabantous, T. Tran, T. C. Terwilliger and G. S. Waldo, *Nat. Biotechnol.*, 2006, **24**, 79.
38 J. K. Takimoto, N. Dellas, J. P. Noel and L. Wang, *ACS Chem. Biol.*, 2011, **6**, 733.
39 S. C. Reddington, A. J. Baldwin, R. Thompson, A. Brancale, E. M. Tippmannk and D. D. Jones, *Chem. Sci.*, 2015, **6**, 1159.
40 H. L. Worthy, H. S. Auhim, W. D. Jamieson, J. R. Pope, A. Wall, R. Batchelor, R. L. Johnson, D. W. Watkins,

P. Rizkallah, O. K. Castell and D. D. Jones, *Commun. Chem.*, 2019, **2**, 83.
41 Z. Xu and S. Y. Lee, *Appl. Environ. Microbiol.*, 1999, **65**, 5142.
42 L. A. Pratt, W. Hsing, K. E. Gibson and T. J. Silhavy, *Mol. Microbiol.*, 1996, **20**, 911.
43 (*a*) I. Calderón, S. R. Lobos, H. A. Rojas, C. Palomino, L. H. Rodríguez and G. C. Mora, *Infect. Immun.*, 1986, **52**, 209; (*b*) Y.-F. Liu, J.-J. Yan, H.-Y. Lei, C.-H. Teng, M.-C. Wang, C.-C. Tseng and J.-J. Wu, *Infect. Immun.*, 2012, **80**, 1815.
44 S. V. Mayer, A. Murnauer, M.-K. von Wrisberg, M.-L. Jokisch and K. Lang, *Angew. Chem., Int. Ed.*, 2019, **58**, 15876.
45 C. D. Spicer, T. Triemer and B. G. Davis, *J. Am. Chem. Soc.*, 2012, **134**, 800.
46 (*a*) K. Kipper, E. G. Lundius, V. Ćurić, I. Nikić, M. Wiessler, E. A. Lemke and J. Elf, *ACS Synth. Biol.*, 2017, **6**, 233; (*b*) A. B. Lindner, R. Madden, A. Demarez, E. J. Stewart and F. Taddei, *Proc. Natl. Acad. Sci. U. S. A.*, 2008, **105**, 3076.
47 M. B. Elowitz, A. J. Levine, E. D. Siggia and P. S. Swain, *Science*, 2002, **297**, 1183.
48 G. Reshes, S. Vanounou, I. Fishov and M. Feingold, *Biophys. J.*, 2008, **94**, 251.
49 A. Rokney, M. Shagan, M. Kessel, Y. Smith, I. Rosenshine and A. B. Oppenheim, *J. Mol. Biol.*, 2009, **392**, 589.
50 J. D. Wang and P. A. Levin, *Nat. Rev. Microbiol.*, 2009, **7**, 822.